correspond to a value of α as defined by relation (5) in the text of 77 °K. If one instead fits to the glass-$Mo_{0.99}Fe_{0.01}$-Pb data, one obtains the value of 148 °K quoted in the text.

[20]A. S. Edelstein, Phys. Rev. 180, 505 (1969).

[21]H. V. Culbert and A. S. Edelstein, Solid State Commun. 8, 445 (1970).

[22]J. S. Kouvel, J. Phys. Chem. Solids 21, 57 (1961).

[23]Y. Miyako, T. Watanabe, and M. Watanabe, Phys. Rev. 182, 495 (1969).

[24]J. A. Careaga, B. Dreyfus, R. Tournier, and L. Weil *Proceedings of the Tenth International Conference on Low Temperature Physics, Moscow, USSR*, 1966 (VINITI Publishing, Moscow, 1967), Vol. IV, p. 284, paper A70.

[25]R. W. Schmitt and I. S. Jacobs, J. Phys. Chem. Solids 3, 324 (1957).

[26]P. G. de Gennes and G. Sarma, J. Appl. Phys. 34, 1380 (1963).

[27]J. J. Hauser, Phys. Rev. Letters 23, 374 (1969).

[28]We are indebted to J. H. Condon for making this experiment.

[29]C. A. Domenicali and E. L. Christenson, J. Appl. Phys. 32, 2450 (1961).

[30]D. R. Hamann, Phys. Rev. B 2, 1373 (1970).

[31]B. T. Matthias, H. Suhl, and E. Corenzwit, Phys. Rev. Letters 1, 92 (1958).

[32]K. H. J. Buschow and H. J. Van Daal, Phys. Rev. Letters 23, 408 (1969).

[33]H. J. Williams, J. H. Wernick, E. A. Nesbitt, and R. C. Sherwood, J. Phys. Soc. Japan Suppl. 17, 91 (1962).

[34]W. M. Swift and W. E. Wallace, J. Phys. Chem. Solids 29, 2053 (1968).

[35]We are indebted to R. C. Sherwood for the magnetic measurements made on $CeAl_2$.

[36]R. W. Hill and J. M. Machado da Silva, Phys. Letters 30A, 13 (1969).

[37]G. J. Van den Berg, in *Progress in Low Temperature Physics*, edited by C. J. Gorter (North-Holland, Amsterdam, 1964), Vol. IV, p. 194.

[38]A. B. Kaiser and M. J. Zuckermann, Phys. Rev. B 1, 229 (1970).

[39]W. L. McMillan, Phys. Rev. 175, 537 (1968).

[40]M. A. Woolf and F. Reif, Phys. Rev. 137, A557 (1965).

[41]J. J. Hauser, Physica 2, 247 (1966).

[42]J. J. Hauser, Phys. Rev. 164, 558 (1967).

[43]A. S. Edelstein, Phys. Rev. Letters 19, 1184 (1967); Phys. Rev. 180, 505 (1969).

[44]T. N. Mihalisin, D. P. Snowden, and P. M. Chaikin (unpublished).

PHYSICAL REVIEW B VOLUME 3, NUMBER 7 1 APRIL 1971

Interaction of 9.3-GHz Longitudinal Phonons with Electrons in Superconducting Films

Moshe Cohen and Y. Goldstein
The Hebrew University, Jerusalem, Israel

and

B. Abeles
RCA Laboratories, Princeton, New Jersey 08540

(Received 2 December 1970)

Previous studies of the interaction of longitudinal phonons with superconducting Al-Pb junctions have been extended to include nonuniform strains, arising when the thicknesses of the metal films are not negligible compared to the wavelength of the sound and/or when the wave front makes a small angle θ with the plane of the junction. It is found that nonuniform strains produce an electric field proportional to the strain gradient inside the "local" superconducting Al film. This result confirms the theories of Dessler *et al.*, Herring, and Harrison who calculated the gravity-induced electric fields. The strain-induced field in the aluminum excites electromagnetic waves in the junction which are enhanced due to the traveling-wave interaction in the strip line formed by the junction. The electromagnetic field gives rise to an extra tunneling current which exhibits resonant behavior as a function of the angle θ. In the "nonlocal" Pb films, the interaction of the electrons with the strain wave is described by absorption and emission of phonons, and the extra tunneling current due to this process is essentially independent of θ. This behavior enables us to separate the extra current due to the Al film and that due to the Pb film. The agreement between theory and experiment is found satisfactory.

I. INTRODUCTION

It was shown several years ago that the interaction between sound waves and electrons in metals can be observed directly by measuring the phonon-induced current in superconducting tunnel junctions.[1-3] In the case of compressional waves,[1,3] this extra current was attributed to a relative motion of the Fermi energies in the two metals due to the compressional strain. In the interpretation of the above experiments it was assumed that the strain was spatially uniform. The present work,

preliminary results of which have recently been reported[4] by the authors, concerns itself with the more general case of a spatially nonuniform strain. The question whether a nonuniform strain gives rise to an electric field outside a metal received considerable attention over the last few years. This interest arose in connection with the attempt of Witteborn and Fairbank[5] to measure the gravitational force acting on an electron. It was pointed out by Dessler *et al.*[6] and Herring[7] that the nonuniform strain set up by gravity in the copper cylinder used in this experiment to shield the electron gives rise to an electric field outside the metal. The force on the electron outside the metal due to this field should have been in the direction of the gravitational force and about four orders of magnitude larger. However, no such force was observed experimentally. To demonstrate directly the presence of an electric field inside a metal due to a nonuniform strain, Beams[8] measured the radial electrical potential gradient across a Duraluminum rotor spinning at high speed. He found a reasonable agreement with the theoretical predictions, but "no clear-cut theoretical interpretation of the experiment was possible." More recently, Craig[9] measured semiquantitatively the effect of uniform stress on the contact potential of several metals. The observed shifts in contact potentials were found to be in order-of-magnitude agreement with the theories that apply for the nonuniform gravitational strain,[6,7] provided one can assume that the gravitational stress is equivalent to a uniform hydraulic stress.

In the present work we treat the case of a nonuniform strain which arises when the thickness of the metal films is not negligible compared to the wavelength of the sound and/or if the wave front is not completely parallel to the film surface. We distinguish between two different cases, $q\xi > 1$ and $q\xi < 1$, where q is the sound wave number and ξ is the Pippard coherence distance.[10] (For a normal metal the above conditions are replaced by $ql \lesssim 1$, where l is the mean free path.) In the case of $q\xi < 1$, local electrodynamics applies and the spatially varying strain produces an electrostatic potential in the metal proportional to the strain.[6,7] A small angle θ between the sound wave vector and the normal to the film results in an extremely fast potential wave in the plane of the film. The velocity of this wave is $v/\sin\theta$, where v is the sound velocity. The potential wave induces electromagnetic waves in the junction, the latter acting as a strip line.[11] When the velocity of the potential wave equals the propagation velocity of an electromagnetic wave in the strip line, resonant coupling occurs due to traveling-wave interaction, and the induced electromagnetic field achieves its maximum amplitude. The presence of the electromagnetic field was detected by its effect on the tunneling current.

In the case $q\xi > 1$, the phonon-electron interaction is described in terms of phonon emission and absorption. The extra tunneling current due to this process has recently been calculated by Cohen.[12] This current is essentially independent of the angle θ, whereas the current due to the electrostatic potential wave is strongly angle dependent. This permitted us to distinguish between the two currents, and to explain an anomaly in the observed magnitude and temperature dependence reported earlier.[3]

II. THEORY

It has been found by Dayem and Martin[13] that the interaction of a microwave electric field with a superconducting tunnel junction gives rise to an extra tunneling current δI. Tien and Gordon[14] calculated this extra current due to a microwave field E across a junction and obtained

$$\delta I = (we/2h\nu)^2 f |E|^2 , \tag{1a}$$

where w is the insulator thickness, h is Planck's constant, and e is the magnitude of the electronic charge. The coefficient f depends on the dc current-voltage (I-V) characteristic of the tunnel junction and on the microwave frequency ν:

$$f = I(V + h\nu) + I(V - h\nu) - 2I(V) . \tag{1b}$$

Equation (1) is valid for fields small enough so that $|E|^2 \ll (h\nu/we)^2$. It was later found that such an extra current can be induced also by compressional sound waves.[1-3] It was shown that for the case of a uniform compressional strain the extra current δI_s is given by Eq. (1), provided that E is replaced by an effective field E_s derived from the difference between the electrochemical potentials of the two metals,

$$E_s = [(sC)_1 - (sC)_2]/we . \tag{2}$$

Here sC is the product of the strain and the deformation potential in the two metals comprising the tunnel junction.

We now proceed to treat the more general case of an extra current due to a spatially nonuniform strain. The geometry we wish to consider is a metal-insulator-metal sandwich on an insulating substrate shown schematically in Fig. 1. We assume that the spatial variation in the strain arises because of the finite thicknesses of the metal films and because of the non-normal incidence of the sound wave. We show here that in this case the sound wave excites an electromagnetic wave in the tunnel junction. The electromagnetic field $\vec{E}$ in the insulator has a component normal to the junction. This component E_x also induces an extra current and has to be added to E_s. Because of the spatial variation of E_x and E_s, δI_s is given now by

$$\delta I_s = (we/2h\nu)^2 (f/a) \int_a |E_x + E_s|^2 \, da \qquad (3)$$

rather than by Eq. (1). The coefficient f in Eq. (3) is still given by Eq. (1b), and the integration is performed over the area a of the junction.

We now proceed to calculate the fields E_s and E_x which enter into Eq. (3). Let the incident acoustic wave propagate in the x-z plane making an angle θ with the positive x direction (see Fig. 1). The wave is totally reflected at the free surface of metal 1, while the other interfaces introduce only partial reflections, insofar as there exists an acoustic mismatch between the respective media. We restrict ourselves to the case of very small angles ($\theta < 1°$), the situation encountered experimentally. In that case the compressional strain s can be expressed in each medium as a product of a running wave in the z direction and a standing wave in the x direction:

$$s(x, z) = s_0 e^{i(\omega t - q_z z)} (e^{-iq_x x} + e^{i(q_x x + \beta)})/(1 + e^{i\beta}) \, . \qquad (4)$$

Here q_x and q_z are the x and z components of the wave vector $\vec{q}$ in each medium, t is the time, and $\omega = 2\pi\nu$. The strain amplitude s_0 and the phase β in the different media are determined by the various reflections. Sound absorption is neglected in Eq. (4), i.e., $\vec{q}$ is real.

The nonuniform strain gives rise to an electrostatic potential φ. At sufficiently low sound frequencies, quasithermal equilibrium is established in each of the metal films and one can define a time varying electrochemical potential. This concept is valid as long as the scale of variation of the electromagnetic field is large compared to the mean free path l, in the case of a normal metal, or the Pippard coherence length[10] ξ, in the case of a superconductor, i.e.,

$ql \ll 1$ for a normal metal,

$q\xi \ll 1$ for a superconductor .

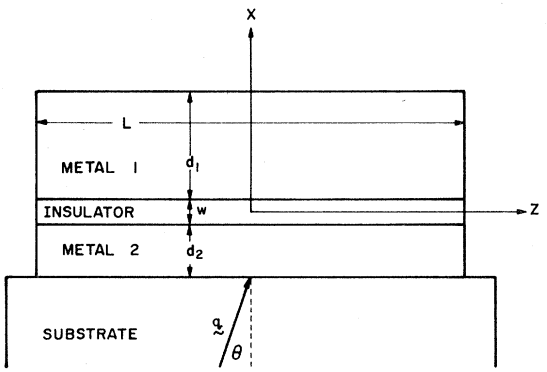

FIG. 1. Schematic representation of tunnel junction. The slightly oblique incidence of the compressional wave is indicated by the wave vector $\vec{q}$.

Here

$$1/\xi = 1/\xi_0 + 1/l \, ,$$

where ξ_0 is the intrinsic coherence length. A lower limit to the frequency is set by the requirement that in order to be able to treat each metal separately, independent of the other metal, we require $\omega\tau \gg 1$, where τ is the capacitive time constant of the junction.[15]

The electrochemical potential μ is defined as

$$\mu = \mu_F - e\varphi \, , \qquad (5)$$

where μ_F is the chemical potential. The electrostatic potential φ is proportional to the difference between s and its average value $\langle s \rangle$ over the volume of the metal,

$$e\varphi = C(s - \langle s \rangle) \, , \qquad (6)$$

where C is defined as the deformation potential. (For a free-electron gas, $C = -\frac{2}{3}\mu_F$.) The chemical potential μ_F is given by

$$\mu_F(s) = \mu_F(0) + Cs \, , \qquad (7)$$

where $\mu_F(0)$ is the chemical potential in the absence of strain.

Substituting Eqs. (6) and (7) into Eq. (5) we obtain for μ

$$\mu(s) = \mu(0) + C\langle s \rangle \, . \qquad (8)$$

The different quantities in Eqs. (5)–(8) are shown schematically in Fig. 2, both in the presence and in the absence of a strain wave. The effective field E_s is given by

$$E_s = (\mu_1 - \mu_2)/we \, . \qquad (9)$$

From this last equation and Eq. (8) it now follows that in the case of a nonuniform strain Eq. (2) for E_s has to be replaced by

$$E_s = [(C\langle s \rangle)_1 - (C\langle s \rangle)_2]/we \, . \qquad (10)$$

We now turn to calculate the electric field E_x in the insulator. It was first pointed out by Pippard[11] that a strip line consisting of a metal-insulator-metal sandwich will propagate an electromagnetic wave but with a reduced velocity. Swihart[11] performed detailed calculations of the electromagnetic propagation constant γ_p of the strip line in terms of the microwave surface impedances of the two metals. The present calculation departs from that of Swihart in that we include the field due to the electrostatic potential φ in each metal. We express the electromagnetic field in the insulator by the vector potential $\vec{\alpha}(x, z, t)$, and we look for solutions of the form

$$\vec{\alpha} = \vec{A}(x) e^{i(\omega t - \gamma z)} \, . \qquad (11)$$

We apply the usual boundary conditions, i.e., the continuity of the parallel components of the electric

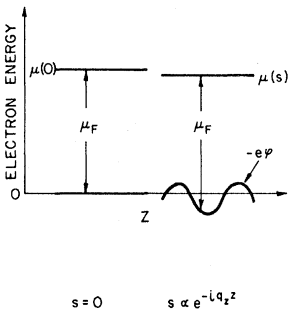

FIG. 2. Schematic representation of the electrochemical potential μ, the chemical potential μ_F, and the electrostatic potential φ, both in the presence and absence of a compressional wave s.

and magnetic fields across the insulator-metal interfaces. We solve the equations for γ and obtain a solution which consists of two characteristic waves propagating in the positive and negative z direction, respectively, with wave number γ_p and a driven wave having the same wave number q_z as the strain. We take into account the finite length L of the strip line in the z direction by requiring the vanishing of the magnetic field at the boundaries $z = \pm \frac{1}{2}L$. From this latter condition we determine the amplitudes of the characteristic waves. The detailed mathematical treatment is given in the Appendix. The solution for E_x is given by

$$E_x = [(Cs_0)_2 - (Cs_0)_1]\, q_z^2 \{ e^{-iq_z z} - (\gamma_p/q_z \sin\gamma_p L)\{\sin[\tfrac{1}{2}(q_z - \gamma_p)L]\, e^{i\gamma_p z} + \sin[\tfrac{1}{2}(q_z + \gamma_p)L]\, e^{-i\gamma_p z}\}\}[we(q_z^2 - \gamma_p^2)]^{-1} , \quad (12)$$

where γ_p is given by Eq. (A19) and we have omitted in Eq. (12) the factor $e^{i\omega t}$.

In the case of $q\xi > 1$, the assumption of quasithermal equilibrium is no longer valid and the interaction of electrons with the sound wave is described via absorption and emission of phonons. This case has been treated theoretically by Cohen,[12] who finds an extra current δI_q with a similar bias and strain dependence as δI_s.

III. EXPERIMENT

The tunnel junctions were vacuum deposited on one end of an X-cut quartz rod. Most of the experiments were done with Al-Pb junctions. An aluminum film a few hundred Å thick was evaporated first, next the film was exposed to dry oxygen at atmospheric pressure for 1 min and then a thick (several thousand Å) lead film was deposited on top. In order to increase the transition temperature of the aluminum films above 2 °K, oxygen was continuously fed into the system during the Al evaporation so as to maintain the pressure at $5-6\times10^{-5}$ Torr.[16] The lead was evaporated at a pressure of 10^{-6} Torr. Typical dimensions of the junctions were 0.1×0.27 cm. The quartz rods were 0.3 cm in diam and 2 cm long with optically polished end faces parallel within 4 sec of an arc. The other end of the quartz rod was inserted into a reentrant microwave cavity. The rod was clamped at a position close to its entrance into the cavity and a bending moment could be applied perpendicular to the axis of the rod by means of three spring loaded Teflon pins situated 120° apart. The arrangement is shown schematically in Fig. 3. The cavity was immersed in liquid helium and the temperature could be varied by reducing the ambient pressure.

The cavity was excited at its resonant frequency $\nu = 9.3$ GHz with 120-W microwave pulses of 1-μsec duration. A microwave pulse produced a compressional sound pulse which propagated along the length of the quartz rod. The measured conversion efficiency of microwave to sound energy was 50 dB. The sound pulse was reflected both at the tunnel junction surface and at the cavity end of the rod and bounced back and forth many times producing a train of sound echoes in the rod. The angle θ_n between the sound wave vector $\vec{q}$ and the normal to the junction is determined by the echo number n and by the angle θ_1 between the end faces of the rod:

$$\theta_n = (2n-1)\,\theta_1 , \quad (13)$$

and the corresponding value of q_z is

$$q_z = q \sin\theta_n \approx q\theta_1(2n-1) . \quad (14)$$

The angle θ_1 could be varied by the application of the bending moment to the rod. Typically the magnitude of θ_1 was less than 60 sec. Coincident with the arrival of the sound echoes at the tunnel junction, an extra tunneling current δI was observed. This current was measured by means of a low-noise pulse amplifier and displayed on an oscilloscope as a function of time. A detailed description of the pulse detection and microwave techniques is given in Ref. 3. Figure 4 shows two typical oscillograms of δI, taken on the same junction, holding the temperature and microwave power constant, but

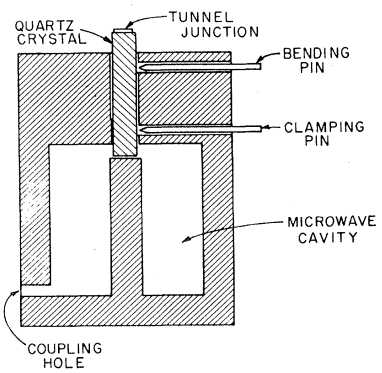

FIG. 3. Schematic representation of the reentrant microwave cavity and the bending arrangment.

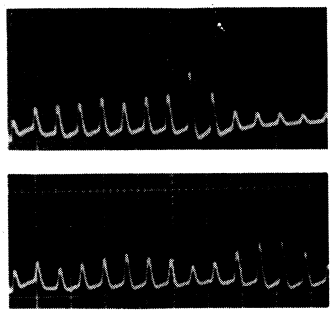

FIG. 4. Two oscillagrams taken on the same junction at constant microwave power and temperature $T = 1.36$ °K. The upper one was taken with a bending moment applied to the quartz rod larger than that for the lower oscillogram. The horizontal scale is 10 μsec/div.

changing the applied bending moment. The dc-voltage bias was set for a maximum δI (see Ref. 4 for the bias dependence of δI). The echo envelopes in both oscillograms exhibit a maximum which occurs at different echo number in each oscillogram. The positions of the maxima were found to be directly related to the applied moments. Increasing the bending moment resulted in a motion of the modulation maximum to lower echo number. In Fig. 5 are plotted the measured amplitudes of δI as a function of echo number n for an Al-Pb junction at various temperatures at constant microwave power and constant applied bending moment. The theoretical lines were fitted to the experimental points as discussed in Sec. IV.

IV. COMPARISON OF EXPERIMENT WITH THEORY

In this section we give a detailed analysis of the data. The aluminum films used in these experiments were granular films[16] with normal resistivities in the range 10^{-5}–10^{-4} Ω cm and coherence distances $\xi_{Al} \approx l \leq 150$ Å. The value of the wave number q in aluminum[17] is $q_{Al} = 9\times10^4$ cm^{-1}, and thus in the case of aluminum, $q\xi \ll 1$ and we expect δI to be given by δI_s. For lead, on the other hand, the coherence distance[10] $\xi_{Pb} = 830$ Å, the wave number[17] $q_{Pb} = 2.9\times10^5$ cm^{-1} and hence $q\xi > 1$. Thus in the case of lead we shall assume that δI is given by δI_q. The total excess current δI is then given by

$$\delta I = \delta I_s(\mathrm{Al}) + \delta I_q(\mathrm{Pb}) \ . \tag{15}$$

The characteristic features of the measured δI (see Fig. 5) is a relatively flat portion at low echo numbers and a pronounced maximum at higher echo numbers. Such a behavior is indeed predicted by the theory. Inspection of Eq. (12) reveals a resonant peak for E_x and via Eq. (3) for δI_s. Thus δI in Eq. (15) consists of a resonant term and a constant contribution via δI_q. The experimentally observed shift of the resonant peak to lower echo numbers with decreasing temperatures is also in agreement with the theoretical predictions. This follows qualitatively from the following facts: The peak in δI occurs at a q_z, which we denote by q_{zm} and which is given approximately by [see Eq. (12)]

$$q_{zm}^2 = \mathrm{Re}(\gamma_p^2) \ . \tag{16}$$

The wave number γ_p can be expressed in terms of the complex conductivity $\sigma = \sigma_1 - i\sigma_2$ [see Eqs. (21) and (A21)]. With decreasing temperature, σ_2 increases, $\mathrm{Re}(\gamma_p^2)$ decreases, and thus n decreases [see Eq. (14)]. We also find that at a fixed temperature the peak shifts to lower echo number with increasing bending moment (see Fig. 4). Increasing the bending moment increases θ_1, and to satisfy Eq. (16) for a fixed γ_p, n has to decrease.

The main discrepancy between theory and experiment is that at larger echo numbers experimentally, δI is observed to decrease, whereas Eq. (15) predicts a constant value. The cause for this discrepancy is that attenuation of the sound beam was not taken into account. The attenuation is primarily due to the fact that by deflecting the sound beam by an angle θ_n, part of the beam is not going to strike the junction area. After each round trip the center of the sound beam is displaced by an amount $4d_0\theta_1$

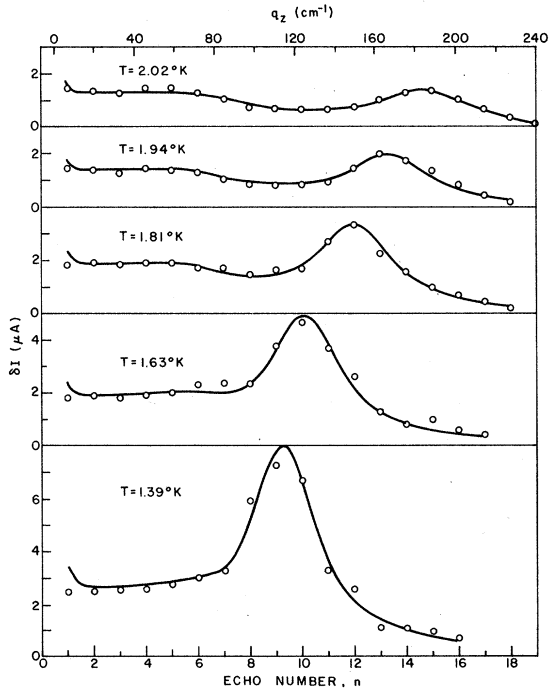

FIG. 5. The extra tunneling current δI for an Al-Pb junction plotted as a function of echo number n (lower scale) and wave number q_z (upper scale) at various temperatures and at constant microwave power and applied bending moment. The experimental results are given by the circles. The theoretical curves were calculated from Eq. (19).

$\times(n-1)$ from its previous position, where d_0 is the length of the crystal. For a bending moment along the y axis, the total displacement z_n along the z direction is given by

$$z_n = 2n(n-1)\, d_0 \theta_1 \,. \tag{17}$$

The junctions used in the experiment were about 0.27 cm long and 0.1 cm wide with the longer dimension along the z axis. The edge of the junction came to about 0.015 cm from the edge of the crystal. As the center of the sound beam is displaced along the z direction, one expects an attenuation in δI once the trailing edge of the beam starts to recede from the junction area. This will occur after the center of the beam is deflected by approximately 0.015 cm. The echo at which this occurs we denote by n_1. After the beam is deflected by an additional 0.27 cm, no sound energy is incident on the junction surface and we expect a cutoff in δI. To allow for this attenuation, δI in Eq. (15) must be multiplied by an attenuation factor $g(n)$. We approximated $g(n)$ by a decreasing exponential for $n > n_1$ and by a constant for smaller n,

$$g(n) = \begin{cases} 1 & \text{for } n \le n_1 \\ e^{-b(n-n_1)} & \text{for } n > n_1 \,, \end{cases} \tag{18}$$

where b is an adjustable parameter. Accordingly we set

$$\delta I = g[\delta I_s(\mathrm{Al}) + \delta I_q(\mathrm{Pb})] \,. \tag{19}$$

Inspection of the data of Fig. 5 shows that up to the sixth echo, δI is essentially unattenuated and accordingly we take $n_1 = 6$. The only temperature-dependent parameters entering the theory are γ_p, $\delta I_q(\mathrm{Pb})$, and f. The coefficient f was determined from the dc I-V characteristics, while the other two were used as parameters in fitting Eq. (19) to the experimental data. The value of the parameter b was found to be 0.21 and $|Cs_0|_{\mathrm{Al}} = 18$ μeV. The theoretical curves are plotted in Fig. 5 as a function of q_z. The proportionality factor between q_z and n [see Eq. (14)], obtained from the fit, is $2q\theta_1 = 13$ cm^{-1}. Writing

$$\gamma_p = \alpha_p (1 - i/Q) \,, \tag{20}$$

we found that the best fit between theory and experiment is obtained using $Q = 9$ independent of temperature. The values of α_p are plotted in Fig. 6 (points) as a function of the reduced temperature T/T_c. The general form of γ_p is given by Eq. (A19) in the Appendix. For the special case of a thin aluminum film, $|K_{\mathrm{Al}} d_{\mathrm{Al}}| \ll 1$, and a thick lead film, $|K_{\mathrm{Pb}} d_{\mathrm{Pb}}| \gg 1$, Eq. (A19) reduces to

$$\gamma_p = (\epsilon\omega^2/c^2)^{1/2}[1 + (i/wK_{\mathrm{Pb}}) + (1/wd_{\mathrm{Al}} K_{\mathrm{Al}}^2)]^{1/2}, \tag{21}$$

where K is given by Eq. (A21). The theoretical curve in Fig. 6 was calculated from Eqs. (21) and (A21) using the values for σ/σ_n from Mattis and Bardeen's theory,[18] where σ_n is the normal conductivity. The thickness of the Al film was approximately 400 Å, its normal conductivity $\sigma_n = 4\times10^4$ Ω^{-1} cm^{-1}, the oxide thickness was estimated to be 20 Å, and ϵ was taken[19] to be 3. The theoretical curve was normalized to the experimental data at $T/T_c = 0.87$. The calculated value of α_p at this temperature was 185 cm^{-1}. Considering the uncertainty in the oxide thickness w and the dielectric constant ϵ, this is in good agreement with the experimental value of $\alpha_p = 173$ cm^{-1}. If we use, on the other hand, the formula for dirty superconductors,[20]

$$\sigma_2/\sigma_n = \left(\frac{1}{0.64}\right)^2 \pi\Delta(0)\,(T_c - T)/T_c h\nu \,, \tag{22}$$

where $\Delta(0)$ is the energy gap of Al at $T = 0$, we obtain $\alpha_p = 191$ cm^{-1}.

The quality factor Q in Eq. (20) is given by $Q \approx 2\sigma_2/\sigma_1$ [see Eqs. (21) and (A21)]. At $T/T_c = 0.87$, the theoretical value of Q is 14 and increases to 54 at $T/T_c = 0.62$. The experimental value of $Q = 9$ indicates that there is an additional contribution to the imaginary part of γ_p.

The fitted values of $\delta I_q(\mathrm{Pb})$ are plotted as a function of temperature in Fig. 7. The observed temperature dependence of $\delta I_q(\mathrm{Pb})$ follows closely that of $f(T)$ and is in reasonable agreement with Cohen's calculations. The magnitude of $\delta I_q(\mathrm{Pb})$ is in an order-of-magnitude agreement with that calculated for Pb-Pb tunnel junctions.[12]

The bending angle θ_1 can be calculated from Eq. (14) and the experimental value of the proportional-

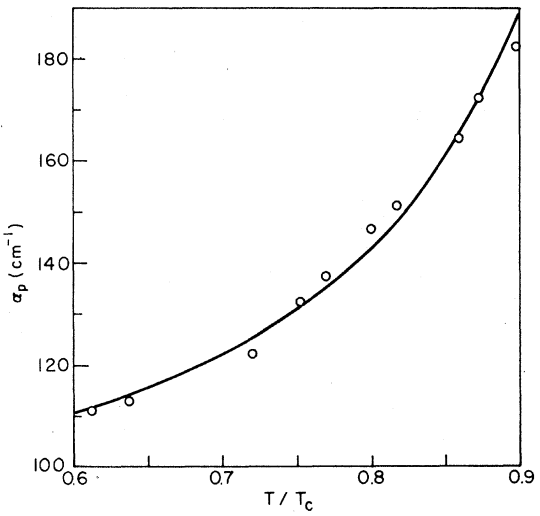

FIG. 6. The real part α_p of the electromagnetic wave number in the strip line as a function of the reduced temperature T/T_c of Al. The circles represent the values used in fitting Eq. (19) to the experimental results in Fig. 5. The transition temperature T_c of Al was 2.26 °K.

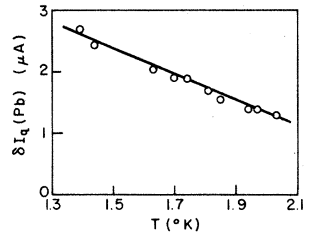

FIG. 7. The extra tunneling current δI_q due to the Pb film as a function of temperature. The circles represent the values used in fitting Eq. (19) to the experimental results in Fig. 5.

ity constant between q_z and the echo number n. The value obtained in this manner is 14.5 sec. Inserting this value for θ_1 into Eq. (17), we can calculate the echo number for which the edge of the sound beam starts to recede from the junction. We obtain that for $z_n = 0.015$ cm, $n = 7.7$. This is consistent with the value of $n_1 = 6$ estimated from Fig. 5.

The theoretical curves exhibit a small decrease going from the first to the second echo. This results from the contribution of E_s to δI_s. The expression for E_s is obtained from Eqs. (4) and (10) and is given by

$$E_s = 4(s_0 C)\sin(\tfrac{1}{2}q_z L)\sin(\tfrac{1}{2}q_x d)/q_x q_z L d\,, \tag{23}$$

where all the relevant quantities apply to Al. At low echo numbers, E_x is negligible, and thus δI_s is dominated by E_s. As E_s enters quadratically into Eq. (3) for δI_s, this contribution to the current will decrease approximately as $\sin^2(\frac{1}{2}q_z)/(\frac{1}{2}q_z L)^2$ and is negligibly small after the first echo. In our measurements we did not resolve this structure.

V. CONCLUSION

The possibility of adjusting the spatial variation of the strain in the films provided, in the present experiments, a means of distinguishing between the phonon-assisted tunneling current δI_q due to the nonlocal superconductor Pb and the strain-induced current δI_s due to the local superconductor Al. The good agreement between the experimental and theoretical results for δI_s provides firm evidence for the existence of an electric field outside the superconducting film proportional to the strain gradient $\partial s/\partial z$. This result is in agreement with the theories of Dressler,[6] Herring,[7] and Harrison[21] developed for the case of gravitation-induced strains, and thus provides an experimental confirmation. The absolute value of the deformation potential, C, in aluminum derived from the experimentally determined $|Cs_0| = 18$ μeV and strain[22] $s_0 = (1-2)\times 10^{-6}$ is 9–18 eV. This value is in reasonable agreement with that deduced from Craig's data and is somewhat higher than the free-electron value of 8 eV.

APPENDIX

To calculate E_x in the insulator we express the electric field $\vec{E}$ and the magnetic field $\vec{H}$ in terms of the vector potential $\vec{\alpha}$ and the scalar potential φ:

$$\vec{E} = -\frac{1}{c}\frac{\partial\vec{\alpha}}{\partial t} - \Delta\varphi\,, \tag{A1}$$

$$\vec{H} = \Delta\times\vec{\alpha}\,, \tag{A2}$$

where we choose the gauge

$$\Delta\cdot\vec{\alpha} = 0\,. \tag{A3}$$

In the two metals φ is given by Eqs. (4) and (6) in Sec. II, while in the insulator $\varphi = 0$. We denote the vector potential $\vec{\alpha}$ in the insulator by $\vec{\alpha}^{(0)}$ and in the two metals by $\vec{\alpha}^{(1)}$ and $\vec{\alpha}^{(2)}$, respectively. After solving for $\vec{\alpha}^{(0)}$ we join the solutions in the different regions so as to satisfy the requirement of continuity of the tangential components of $\vec{E}$ and $\vec{H}$. In the insulator $\vec{\alpha}$ is determined from the wave equation

$$\nabla^2\vec{\alpha}^{(0)} = \frac{\epsilon}{c^2}\frac{\partial^2\vec{\alpha}^{(0)}}{\partial t^2}\,, \tag{A4}$$

where ϵ is the dielectric constant of the insulator. We seek wavelike solutions in the z direction of the form

$$\vec{\alpha}^{(0)}(x,z,t) = \vec{\alpha}^{(0)}(x)e^{i(\omega t-\gamma z)}\,, \tag{A5}$$

and because of the symmetry of the problem we take $\alpha_y = 0$. Substituting $\vec{\alpha}^{(0)}$ from Eq. (A5) into Eq. (A4) yields

$$\frac{d^2\vec{\alpha}^{(0)}}{dx^2} - \Gamma^2\vec{\alpha}^{(0)} = 0\,, \tag{A6}$$

where

$$\Gamma^2 = \gamma^2 - (\epsilon\omega^2/c^2)\,. \tag{A7}$$

The general solution of Eq. (A6) is given by

$$\vec{\alpha}^{(0)}(x) = \vec{R}\,e^{-\Gamma x} + \vec{S}\,e^{\Gamma x}\,, \tag{A8}$$

where the vectors $\vec{R}$ and $\vec{S}$ are integration constants. In order to satisfy Eq. (A3), the components of $\vec{R}$ and $\vec{S}$ must satisfy the relations

$$R_x = -i(\gamma/\Gamma)R_z\,, \tag{A9}$$

$$S_x = i(\gamma/\Gamma)S_z\,. \tag{A10}$$

Using Eqs. (A1) and (A2), the conditions of the continuity of the tangential components of $\vec{E}$ and $\vec{H}$ across the metal-insulator boundaries ($x = \pm\frac{1}{2}w$) lead to the four relations

$$\left.\begin{aligned} \mathfrak{a}_z^{(0)} &= \frac{c}{i\omega}\frac{\partial\varphi^{(1)}}{\partial z} + \mathfrak{a}_z^{(1)} \\ [\nabla\times\vec{\mathfrak{a}}^{(0)}]_y &= [\nabla\times\vec{\mathfrak{a}}^{(1)}]_y \end{aligned}\right\} x = \tfrac{1}{2}w \,, \tag{A11, A12}$$

$$\left.\begin{aligned} \mathfrak{a}_z^{(0)} &= \frac{c}{i\omega}\frac{\partial\varphi^{(2)}}{\partial z} + \mathfrak{a}_z^{(2)} \\ [\nabla\times\vec{\mathfrak{a}}^{(0)}]_y &= [\nabla\times\vec{\mathfrak{a}}^{(2)}]_y \end{aligned}\right\} x = -\tfrac{1}{2}w \,, \tag{A13, A14}$$

where $\varphi^{(1)}$, $\varphi^{(2)}$ are the electrostatic potentials in metals 1, 2, respectively. In the metals the ratio $\mathfrak{a}_x/\mathfrak{a}_y$ is of the order of $|\gamma/K|$, where K is the wave number of the electromagnetic wave in the metal. This follows from Eq. (A3) and the fact that in the metals $\mathfrak{a} \sim \exp[-i(Kx+\gamma z)]$. For the case treated here this ratio is negligible and thus to a very good approximation

$$\mathfrak{a}_z^{(1)}/(\nabla\times\vec{\mathfrak{a}}^{(1)})_y = (ic^2/4\pi\omega)Z_1 \,, \quad x = \tfrac{1}{2}w \tag{A15}$$

$$\mathfrak{a}_z^{(2)}/(\nabla\times\vec{\mathfrak{a}}^{(2)})_y = -(ic^2/4\pi\omega)Z_2 \,, \quad x = -\tfrac{1}{2}w \,, \tag{A16}$$

where Z_1 and Z_2 are the microwave surface impedances of the two metals. Combining Eqs. (4), (6), and (A9)–(A16) results in the two linear equations for R_z and S_z:

$$R_z\left(1+\frac{i\epsilon\omega Z_1}{4\pi\Gamma}\right)e^{-\Gamma w/2} + S_z\left(1-\frac{i\epsilon\omega Z_1}{4\pi\Gamma}\right)e^{\Gamma w/2} = -q_z(Cs_0)_1\frac{c}{e\omega}e^{i(\gamma-q_z)z} \,, \tag{A17}$$

$$R_z\left(1-\frac{i\epsilon\omega Z_2}{4\pi\Gamma}\right)e^{\Gamma w/2} + S_z\left(1+\frac{i\epsilon\omega Z_2}{4\pi\Gamma}\right)e^{-\Gamma w/2} = -q_z(Cs_0)_2\frac{c}{e\omega}e^{i(\gamma-q_z)z} \,. \tag{A18}$$

In deriving the last two equations we have neglected the small phase shift $e^{iqw/2}$ across the insulator because $wq \ll 1$. Furthermore, since $w\Gamma \ll 1$, we shall in Eqs. (A17) and (A18) expand the factor $e^{\pm\Gamma w/2}$ and retain only the first two terms.

The characteristic wave numbers of the strip line γ_1 and γ_2 are determined from the roots of the equation $|D(\Gamma)| = 0$, where $|D(\Gamma)|$ is the determinant of the left-hand side of Eqs. (A17) and (A18):

$$\gamma_1^2 = \gamma_2^2 = \gamma_p^2 = (\epsilon\omega^2/c^2)[1 + ic^2(Z_1+Z_2)/4\pi w\omega] \,, \tag{A19}$$

where we have neglected $(\epsilon\omega/4\pi\Gamma)^2 Z_1 Z_2$ with respect to unity. The microwave surface impedance Z of a metal film is given by

$$Z = 4\pi\omega\coth(iKd)/Kc^2 \,, \tag{A20}$$

where d is the film thickness and K is the wave number of the electromagnetic wave. In terms of the complex conductivity σ, the wave number K can be expressed as

$$K^2 = 4\pi i\omega\sigma/c^2 \,. \tag{A21}$$

The wave excited by the sound is obtained by looking for a particular solution of Eqs. (A17) and (A18). We set $\gamma = q_z$ and solve for R_z and S_z. Substituting these values into Eqs. (A8)–(A10) we obtain $A_x^{(0)}$. Using Eqs. (A1) and (A5) we obtain

$$E_x' = [(Cs_0)_2 - (Cs_0)_1]q_z^2\exp(-iq_z z)/we(q_z^2 - \gamma_p^2) \,. \tag{A22}$$

Here we have neglected the small variation of E_x' with x within the oxide layer. The complete solution for E_x is given by the sum of E_x' from Eq. (A22) and the characteristic waves $E_1 e^{i\gamma_p z} + E_2 e^{-i\gamma_p z}$. The two coefficients E_1 and E_2 are determined by the requirement that $\vec{H}^{(0)}$ vanish at the two ends of the strip line $z = \pm\frac{1}{2}L$. This is the proper boundary condition for an open-ended strip line. The resulting expression for E_x is given by Eq. (12) in Sec. II.

[1] E. Lax and F. L. Vernon, Jr., Phys. Rev. Letters 14, 256 (1965).

[2] Y. Goldstein and B. Abeles, Phys. Letters 14, 78 (1965).

[3] B. Abeles and Y. Goldstein, Phys. Rev. Letters 14, 595 (1965); Y. Goldstein, B. Abeles, and R. W. Cohen, Phys. Rev. 151, 349 (1966).

[4] Y. Goldstein, M. Cohen, and B. Abeles, Phys. Rev. Letters 25, 1571 (1970).

[5] F. C. Witteborn and W. M. Fairbank, Phys. Rev. Letters 19, 1049 (1967); Nature 220, 436 (1968).

[6] A. J. Dessler, F. C. Michel, H. E. Rorschach, and G. T. Trammell, Phys. Rev. 168, 737 (1968).

[7] C. Herring, Phys. Rev. 171, 1361 (1968).

[8] J. W. Beams, Phys. Rev. Letters 21, 1093 (1968).

[9] P. P. Craig, Phys. Rev. Letters 22, 700 (1969).

[10] For definition and values of ξ see, for instance, P. G. DeGennes, *Superconductivity of Metals and Alloys* (Benjamin, New York, 1969).

[11] James C. Swihart, J. Appl. Phys. 32, 461 (1961); A. B. Pippard, Proc. Roy Soc. (London) A191, 385, (1947); A191, 399 (1947); see also P. V. Mason and R. W. Gould, J. Appl. Phys. 40, 2039 (1969).

[12] R. W. Cohen, Phys. Letters A33, 271 (1970).

[13] A. H. Dayem and R. J. Martin, Phys. Rev. Letters 8, 246 (1962).

[14] P. K. Tien and J. P. Gordon, Phys. Rev. 129, 647 (1963).

[15] The capacitive time constant is $\tau = \epsilon r a/4\pi w$, where r is the tunneling resistance, and the remaining quantities are defined in the text. Substituting for the above quantities from Sec. III and IV and using a typical value $r = 5\ \Omega$, we calculate $\tau \approx 10^{-7}$ sec and thus $\omega\tau \approx 10^4$.

[16] Details of the preparation of the granular aluminum films and their normal and superconducting properties are given by R. W. Cohen and B. Abeles, Phys. Rev.

168, 444 (1968).
[17]Calculated from the elastic constant C_{11} of aluminum, P. M. Sutton, Phys. Rev. 91, 816 (1953); and lead, E. H. Swift and E. P. T. Tyndall, *ibid.* 61, 359 (1942).
[18]D. C. Mattis and J. Bardeen, Phys. Rev. 111, 412 (1958).
[19]We have determined ϵ from the index of refraction of Al_2O_3 given in *American Institute of Physics Handbook* (McGraw-Hill, New York, 1957), Chap. 6, p. 24.
[20]Equation (22) is derived by expressing in Eq. (A21) the quantity K in terms of the penetration depth of a dirty superconductor (see, for instance, Ref. 10, p. 225).
[21]W. A. Harrison, Phys. Rev. 180, 1606 (1969).
[22]The strain s_0 was determined from the measured conversion efficiency of microwave power to acoustic power. The uncertainty in s_0 reflects the uncertainty in the conversion efficiency.

PHYSICAL REVIEW B VOLUME 3, NUMBER 7 1 APRIL 1971

"Intermediate Mixed" State of Type-II Superconductors*

D. R. Aston† and L. W. Dubeck
Physics Department, Temple University, Philadelphia, Pennsylvania 19122

and

F. Rothwarf
Pitman-Dunn Laboratories, Frankford Arsenal, Philadelphia, Pennsylvania 19137

(Received 2 March 1970)

For magnetic fields in the range $(1-D)H_{c1} < H < H_t$, magnetization curves of low-κ type-II Pb-In and In-Bi alloys with nonzero demagnetization coefficients D exhibit a linear dependence of the magnetic moment on applied field. H_{c1} is the lower critical field and H_t is the field at which this linear dependence terminates. For finite D, $H_t < H_{c1}$. This behavior can be explained by a model of alternate regions of superconducting and mixed states. This array may be metastable. The mixed-state regions are all presumed to have the same temperature-dependent fluxoid-lattice spacing characteristic of H_{c1} when $D=0$. Thus, as the magnetic field is increased isothermally, the mixed-state regions grow until the whole sample has been converted into the mixed state. This model implies the existence of an attractive interaction between flux lines in low-κ materials.

I. INTRODUCTION

In a recent systematic study[1] of the effects of the demagnetization coefficient D on the magnetization curves of Pb-In and In-Bi alloys, we have verified the Cape-Zimmerman[2] equation

$$-4\pi(dM/dH)_{H_{c2}} = [\beta(2\kappa_2^2 - 1) + D]^{-1} , \quad (1)$$

where β is a constant taken to be 1.16 for a triangular flux lattice[3] and κ_2 is the generalized Ginzburg-Landau (GL) parameter. Another generalized GL parameter κ_1 was also obtained as a function of temperature and composition by using the Maki[4] results

$$H_c = H_{c2}/(\sqrt{2}\kappa_1) , \quad (2)$$

where H_c is the thermodynamic critical field and H_{c2} is the upper critical field. Our measurements also indicated that $\kappa_1 = \kappa_2$ for all compositions and temperatures studied, in agreement with the results of Kinsel, Lynton, and Serin[5-7] for In-Bi alloys with $D=0$. In the course of this work, we observed an "intermediate-state-like" behavior, similar to that seen in type-I superconductors, which is illustrated in Fig. 1. Both the low-κ Pb–2 at.% In and In–1.5 at.% Bi samples undergo an isothermal transition from type-I intermediate-state-like behavior to type-II behavior as the applied magnetic field is increased above some characteristic field H_t. This should not be confused with the observations of Kinsel *et al.*[5-7] on an In–1.5 at.% Bi sample which at higher temperatures exhibited type-I characteristics, but at lower temperatures demonstrated type-II behavior. Both of our samples also exhibited exclusively type-I behavior near T_c. At lower temperatures, the samples are type II for $D=0$ (i.e., $\kappa > 0.71$). However, for a finite D they exhibit intermediate-state-like behavior over a certain region of applied field, i.e., $(1-D)H_{c1} < H < H_t$, where H_{c1} is the lower critical field and H_t is the field at which the sample has fully transformed into the mixed state. As we shall show below, $H_t < H_{c1}$ for finite D. Kinsel *et al.*[5-7] did not observe this latter effect because their samples were measured in a longitudinal field and thus demagnetization effects were absent.

There are electron-microscope measurements on these and similar alloy systems which bear directly on the interpretation of our macroscopic magnetization measurements. Thus, it is neces-

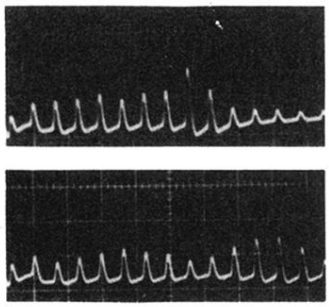

FIG. 4. Two oscillagrams taken on the same junction at constant microwave power and temperature $T = 1.36\,^{\circ}\mathrm{K}$. The upper one was taken with a bending moment applied to the quartz rod larger than that for the lower oscillogram. The horizontal scale is 10 μsec/div.